In vivo optical imaging of physiological responses to photostimulation in human photoreceptors

Dierck Hillmann,^{1,*} Hendrik Spahr,^{2,3} Clara Pfäffle,^{2,3} Helge Sudkamp,^{2,3} Gesa Franke,^{2,3} Gereon Hüttmann^{2,3,4}

¹Thorlabs GmbH, Maria-Goeppert-Straße 9, 23562 Lübeck, Germany

²Institute of Biomedical Optics Lübeck, Peter-Monnik-Weg 4, 23562 Lübeck, Germany

³Medical Laser Center Lübeck GmbH, Peter-Monnik-Weg 4, 23562 Lübeck, Germany

⁴Airway Research Center North (ARCN), Member of the German Center for Lung Research (DZL), Germany

*dhillmann@thorlabs.com

Non-invasive functional imaging of molecular and cellular processes of vision is expected to have immense impact on research and clinical diagnostics. Although suitable intrinsic optical signals (IOS) have been observed ex vivo and in immobilized animals in vivo, it was so far not possible to obtain convincing IOS of photoreceptor activity in humans in vivo. Here, we observed spatially and temporally clearly resolved changes in the optical path length of the photoreceptor outer segment as response to an optical stimulus in living human. To obtain these changes, we evaluated phase data of a parallelized and computationally aberration-corrected optical coherence tomography (OCT) system. The noninvasive detection of optical path length changes shows the neuronal photoreceptor activity of single cones in living human retina, and, more importantly, it provides a new diagnostic option in ophthalmology and neurology and could give new insights into

visual phototransduction in humans.

Spatially resolved optical detection of retinal function in living humans promises new diagnostic possibilities and new insights into in vivo phototransduction. Vision starts with the photoabsorption by the "visual purple" rhodopsin or an equivalent photopsin in retinal photoreceptors, which triggers an amplifying biochemical chain reaction finally leading to hyperpolarization of the cell and signaling to the brain - a process known as visual phototransduction. In addition to initial bleaching of rhodopsin itself, several optical changes arise during this vision process (e.g., ^{1,2}) and in the past decades, this led scientists to investigate intrinsic optical physiological responses to retinal photostimulation ex vivo and in animals in vivo by various optical techniques, e.g., microscopes, fundus cameras, and laser scanning ophthalmoscopes (reviewed in³). In fact, different fast intrinsic optical signals after light stimulus were reported, visible as changes in light scattering, absorption, or birefringence, with time constants from milliseconds to seconds. The best in vivo results have been weak signals, obtained by merely looking at the backscattering intensity. In humans, however, these signals were disturbed by rapid eye motion³⁻⁸ and could therefore not be reliably detected.

Principally, optical coherence tomography (OCT⁹) offers unique advantages for the observation of intrinsic optical signals, as it provides three-dimensional infrared imaging of backscattered light, and thereby achieves precise signal localization and minimizes additional undesired photostimulation. Almost ten years ago weak changes in backscattering intensity after retinal stimulation were observed using OCT *in vitro*¹⁰ and in animals.¹¹ As with other imaging tech-

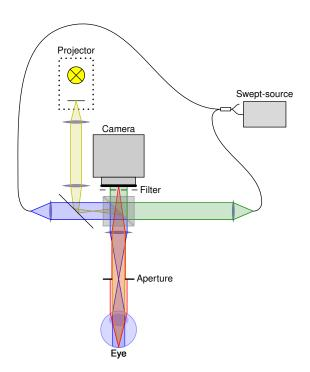


Figure 1: Setup used to observe intrinsic optical signals. Light from a tunable laser source is split in two beams for reference irradiation (green) and illumination of the retina (blue). Backscattered light (red) is imaged onto an a fast CMOS camera, where it is superimposed with the reference light. A projector with an LED source is used to stimulate the retina (yellow).

niques, published studies in humans had significant problems with motion, resulting in even weaker signals, and were not able to convincingly demonstrate the measurement of intrinsic optical signals.^{6–8}

In addition to backscattering intensity, state-ofthe-art Fourier-domain OCT (FD-OCT) also detects phases, which are sensitive to small changes of the optical path length that the backscattered light has travelled. The optical path length of the photoreceptor outer segment is proportional to the time light requires to pass the cells, and it reflects morphology and refractive index, which principally both could be affected during phototransduction. Still, so far no study concentrated on the phase signal to observe fast intrinsic optical signals: to achieve sufficient motion stability for a detection of small phase changes in vivo, the requirements in imaging speed are enormous. Fully parallelized OCT techniques, such as holoscopy¹² and full-field swept-source OCT (FF-SS-OCT),^{13,14} can principally acquire data significantly faster. Recently, FF-SS-OCT thereby detected heartbeat induced pressure waves within retinal vessels¹⁵ and imaged single photoreceptors by using computa-

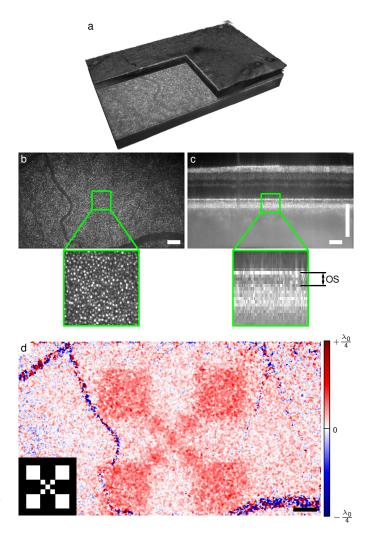


Figure 2: Retinal imaging and response to optical stimulus. a) Volume of retina acquired by full-field swept-source OCT. b) En-face plane showing the backscattering intensity from the outer segment. Cone photoreceptors are clearly visible. c) Cross-sectional view (B-scan) from the center of the recorded volume. Changes of the optical path length within the outer segment (OS) were evaluated in this study. d) Spatially resolved change of the optical path length $\Delta\ell$, 297 ms after the stimulus pattern, which is shown in lower left inset. Response is high in the stimulated region and random in blood vessels. Noise was reduced by a lateral Gaussian filter. The center wavelength λ_0 of the OCT was 841 nm. Scale bars are 200 μ m.

tional aberration correction. 16-18

Here, we measured changes of the optical path length $\Delta\ell$ within the photoreceptor outer segment after projecting a 50 ms white light pattern with a total radiant flux of 10 μ W onto the retina of a healthy young adult. For this, we imaged the retina before, during, and after the stimulus using a FF-SS-OCT sys-

tem (Fig. 1) with up to 180 volumes/s – significantly faster than other OCT systems in research. We then reconstructed the acquired volumes, corrected them for motion, segmented the inner segment/outer segment layer, and flattened it. Figure 2a shows a resulting imaged volume from the periphery at about 11°. After correcting the data numerically for ocular aberrations, cone photoreceptors in the en face images (Fig 2b) become clearly visible. When evaluating phase difference changes between the photoreceptor inner segment/outer segment junction and the outer segment tips (see sectional view (B-scan) in Fig. 2c), we observed an increase of about 50 nm in the optical path length within the outer segment, 297 ms after beginning of the stimulus (Fig. 2d). The signal is clearly related to the stimulus as spatial correspondence to the projected pattern was obvious (bottom left inset of Fig. 2d). However, since the optical path length is the product of the refractive index and the geometric length, we cannot differentiate between chemical and structural changes.

We derived the timecourse of the signals from a series of 70 consecutive volumes acquired at a rate of 180 Hz to provide a temporal resolution of 6 ms and another series acquired at 20 volumes/s for a measurement of more than 3 s, respectively; in both cases the 50 ms stimulus started at the beginning of the 10th volume. After averaging the stimulated area (Fig. 3e,f), we observed the optical path length of the outer segments $\Delta \ell$ to decrease by 5 nm during the first 15 ms of the stimulus. However, the signal was weak and required averaging of 7 measurements to become clearly visible. After these 15 ms, the optical path length started to increase significantly, even several hundred milliseconds beyond the end of the stimulus (Fig. 3e). After about 300 ms the signal reaches its maximum of 40 nm, then dropped for 2.5 s with almost constant rate back to the ground level (Fig. 3f). Figures 3a-d show images from this time series.

Bleaching of rhodopsin and activation of metarhodopsin II happens in the order of a few milliseconds,¹ and the initial response might therefore be related to the direct photoactivation. In *ex vivo* experiments with bovine rod outer segments, rapid disc shrinkage after light exposure was in fact previously reported.¹⁹ The following increase of the optical path length within the outer segment lasts significantly longer than the stimulus, which indicates the signal follows activation of metarhodopsin II and therefore

might be related to its deactivation, follows the activation of transducin, or is related to other secondary processes. Non-physiologic effects, such as a thermal expansion, would cause a direct decrease once the stimulus stops²⁰ and can therefore be ruled out. In addition, we expect hemodynamic changes to last longer than a few 100 ms and not to be this highly localized.

Amplitude and timecourse of the signal depended on stimulus intensity, as its attenuation by OD 0.3 (factor 0.5) and OD 1.3 (factor 0.05) filters showed (Fig. 3k). The optical path length of the outer segment rose with a rate independent of the illumination strength, however, the maximum change increased with stimulus intensity. The increase rate of most photoproducts such as transducin or phosphodiesterase is proportional to the actual stimulation strength, as suggested by kinetic evaluations;²¹ consequently, the observed effect cannot be directly related to these photoproducts. This corroborates our hypothesis of a secondary more complicated effect being responsible for this signal.

Finally, we enlarged the response by using longer stimuli (Figs. 3g-j,l). With a permanent stimulus, the increase of the optical path length of the outer segment was more than 400 nm after 3 s. Here, the optical path length increased even by more than a quarter of the detection wavelength, $\lambda_0/4\approx 210\,\mathrm{nm}$, and the phase differences exceeded π and phase wrapping to $-\pi$ occurred. This resulted in the visible abrupt change from $+\lambda_0/4$ to $-\lambda_0/4$ in Figs. 3i,j. Additionally, in Figs. 3h-j an increased signal background is visible, which is likely caused by a limited stimulus contrast.

Using such strong responses, we were able to assign the signals at the end of the series to single cone photoreceptors; however, a temporal filter needed to be applied and the phase data had to be unwrapped to improve signals first. Figure 4 maps the response on the en face intensity image. One can see, that although most cones reacted to the stimulus, some exhibited only a small or no response. Imaging was sufficiently reproducible to study individual cones over time, and a measured dataset 10 minutes later showed the same cones not contributing (Fig. 4a,b). One can also see that in some locations the phase changed abruptly within a single cone, which might indicate insufficient resolution to resolve all contributing structures. In the presented field of view we were only able to see the

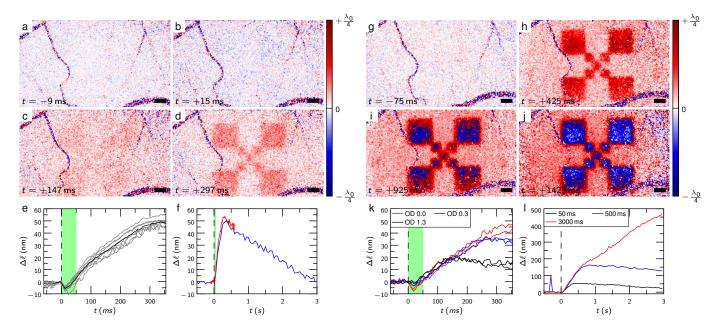


Figure 3: Timecourse of the intrinsic optical signal $\Delta\ell$ for different stimuli. a-d) Response to a 50 ms stimulus; a small negative response after about 17 ms (b) converts to a strong positive stimulation (c-d). e,f) Timecourse, averaged over the stimulated area. The black line (e) is the average of 7 individual measurements (gray lines). g-j) Response to a permanent stimulus. An increasing response is observed, finally leading to phase wrapping. k) Response to different flash intensities attenuated by OD 0.3 and OD 1.3, respectively. I) Response for 50 ms, 500 ms, and 3000 ms stimuli with 10 μ W. The dashed black lines indicate the start of the stimulus at t=0 (e,f,k,l), the green areas (e,f,k) indicate the duration of the stimuli. The center wavelength λ_0 of the OCT was 841 nm. Scale bars are 200 μ m.

cones and unresolvable, smaller rods might have contributed to the observed phases. The same procedure can also be used for other, more complicated stimulus patterns and shows which photoreceptors contribute to the image seen by the test person (Fig. 4c).

The key to our observations is certainly the analysis of the optical path length changes in the outer segments, which was achieved by the enormous measurement speed and related phase stability of FF-SS-OCT. We expect further enhancements in the registration and segmentation of the data to improve the overall signal quality as well. No principle reason exists why fast scanning OCT systems cannot obtain comparable results, assuming that sufficient phase stability is established. The OCT system used in our experiments has a comparably low axial resolution which is limited by the availability of suitable lasers; higher axial resolution would result in better separation of retinal layers, which might not only show a more precise physical origin of the signal, but would likely also enhance signal quality. Nevertheless, all results presented here were highly reproducible; measurements within a few hours gave almost identical timecourses, and only longer breaks resulted in slightly different overall amplitudes, but showed qualitatively similar behaviour.

The method presented here resolved small changes within the optical path length of the outer segment. For backscattered light contributing to an image, these changes cause a fluctuation in image intensity as the light interferes. Jonnal et al. even observed an alternating reflection signal from individual cones and suggested that this might be caused by a change in the optical path length within the outer segment.⁴ Depending on resolution and imaging method, these changes might appear random and in fact previous studies reported variations in sign and magnitude of observed backscattering intensity signals.^{3,6,8}

Currently, we do not know the cause of the observed signal, and further research is required to identify the origin or show its pathology-related value in clinical trials. Nevertheless, detecting the activity of single cones could be an important tool in early diagnostics of many diseases that are known to be associated with loss of photoreceptor function, e.g., agerelated macular degeneration²² and retinitis pigmentosa.²³ In addition, the functional loss of single neuronal photoreceptors might also be an indicator for

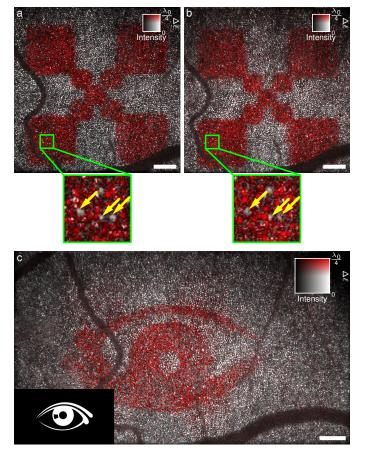


Figure 4: After numerical aberration correction optical path length changes $\Delta\ell$ can be assigned to single cones. a,b) Independent responses to 3 s light stimulus were measured about 10 min apart. Due to the high lateral resolution individual photoreceptors can be identified. Here, the same cones did do not respond to the stimulus (yellow arrows). c) More complicated stimulation patterns can be identified, and show which photoreceptors contribute to an image. The pattern of activated photoreceptors is mirrored compared to the stimulus pattern. The center wavelength λ_0 of the OCT was 841 nm. Scale bars are 200 μm .

neurodegenerative diseases, such as Parkinson's²⁴ or Alzheimer's disease, e.g., the latter degenerates the retinal ganglion cells,²⁵ but with the proposed technique one could also investigate its effect on photoreceptor function.

Methods

Setup The setup consisted of a full-field swept-source optical coherence tomography system (FF-SS-OCT) with an LCD based projection system to stimulate the retina (Fig. 1). A cold mirror coupled the

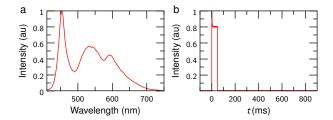


Figure 5: Characteristics of the flash used to simulate the retina. a) Spectrum of the flash. b) Intensity of a 50 ms flash as a function of time, measured using a photodiode.

projection light (yellow in Fig. 1) into the sample illumination arm of the OCT system (blue in Fig. 1) and an infrared long pass filter in front of the camera ensured that no visible light of the stimulation disturbed the OCT system.

The FF-SS-OCT system used a tunable light source (Superlum Broadsweeper BS-840-1), which was connected via a fibre coupler to the reference and to the sample arm of the interferometer. The reference arm illuminated the camera (Photron FastCAM SA-Z) with a parallel beam through a beam splitter (green in Fig. 1), whereas the sample arm illuminated an area of about $3.6 \times 1.5\,\mathrm{mm}$ on the retina through a suitable lens system (blue in Fig. 1). The total radiant flux on the retina from the sample illumination was about $5\,\mathrm{mW}$. The light backscattered by the retina was imaged onto the camera (red in Fig. 1) where it was superimposed with the reference light. An iris controlled the aperture of the retinal imaging to ensure correct sampling of all lateral frequencies by the camera.

A single volume was acquired by obtaining multiple images while tuning the wavelength of the laser. In general, the laser was tuned from 867 to 816 nm, which results in an axial resolution (full width at half maximum) of 8.5 μ m in air, when considering its rectangular spectrum. During the wavelength scan the camera acquired 380 or 512 images, 640 \times 368 pixels each, with 75,000 or 60,000 frames per second, respectively. Depending on the imaging requirements, acquisition speed thereby corresponded to 48.8 MHz Ascan-rate or 29.0 MHz A-scan rate, the maximum volume rates were 180 Hz or 120 Hz, respectively.

To project the image onto the retina, an LED LCD projector was modified with an external microprocessor board (Arduino UNO), which controlled the LED and synchronized the stimulus with the OCT sys-

tem, i.e., it triggered the camera and the tunable laser source. The LCD was imaged via a set of lenses into the conjugate plane of the retina in the sample illumination arm. Spectrum and timecourse of the white light retina illumination light were checked carefully and can be found in Fig. 5.

Additionally, a passive fixation target and a mesh plastic face mask were used for optimal imaging. While the fixation target was illuminated with a green LED to make it visible for the volunteer, care was taken that no green light of the fixation target was visible in the area measured by OCT and illuminated by the projector. The mask was custom fit to the volunteer, ensured a steady and repeatable position of his head, and made imaged areas highly reproducible.

Measurement The area that can be read out is limited by the lateral resolution and by the required camera frame rate. Additionally, blood vessels shadow the outer segment. Therefore, we chose a part of the retina with few blood vessels, and where cones could be resolved after aberration correction. Before the first measurement, the volunteer's pupil was medically dilated and the volunteer was kept in the dark for about 20 minutes, which ensured a reproducible starting point for all measurements, although measurements with normal light adaption (not presented here) gave comparable results. Additionally, sufficient time of at least 5 min in between single measurements ensured that results were not influenced by previous stimulations.

All investigations were done with healthy volunteers; written informed consent was obtained from all subjects. Compliance with the maximal permissible exposure (MPE) of the retina and all relevant safety rules was confirmed by the responsible safety officer. The study was approved by the ethical board of the University of Lübeck (ethical approval "Ethik-Kommission Lübeck 16-080").

Pre-processing After acquiring the raw images of the camera and before evaluating the actual phases, the acquired data was pre-processed: First, the volumetric OCT data for each volume within a time series was reconstructed. To reduce fixed artifacts within the image, the sum of all datasets was computed and then subtracted from all volumes within the dataset, which effectively removed fixed pattern noise as only

the retina changes due to eye motion in between volumes. Afterwards, a Fourier transform along the time axis for each pixel of the camera reconstructed the depth information, i.e., intensity and phase of the volume. Lateral frequency filtering removed noise from outside the aperture and slightly improved signal-tonoise ratio.

Second, the images were corrected for dispersion mismatch in reference and sample arm, as well as intra and inter volume motion. For this, an optimization algorithm^{18,26} removed the influence of dispersion and axial motion in order to obtain sharp OCT volumes. All volumes within a series were then shifted in all three dimensions to maximize their correlation and remove inter volume displacements.

In the next step the inner segment/outer segment junction (IS/OS) of the reconstructed series was segmented independently for each volume. We shifted all A-scans within each volume axially by using the Fourier shift theorem such that the IS/OS appeared to be in a single depth. This ensured reproducible starting conditions for the following step and the final phase evaluation.

Finally, the volume was corrected for ocular aberrations in the segmented layer. The aberration correction of the IS/OS layer made single cone photoreceptors resolvable¹⁷ and was done by an optimization procedure. The algorithm varied Zernike polynomials, which parameterized the aberrations, until an image quality metric (Shannon's entropy²⁷) was optimal. As aberrations varied laterally, the image field was separated into different areas, which were corrected independently and later stitched back together. Although this step improved resolution to resolve individual cones, it was not required to actually observe the changes in the optical path length within the outer segment.

Calculation of the optical path length changes from the measured phases The detected phases in FD-OCT do not carry information on absolute position and to obtain changes, they need to be referenced to phases in other layers and at other times. To cancel this arbitrary phase offset in each pixel the reconstructed volumes f_{xyzt} were first referenced to the last complete volume f_{xyzt} before the stimulus began

$$f_{xyzt}^{(1)} = f_{xyzt} f_{xyzt_0}^*,$$

where x, y, and z denote the spatial indices of the volume, and t is the volume number and corresponds to the recording time. The signal was then averaged over the three layers next to the boundaries of the outer segment by computing the mean of the complex numbers, i.e., the mean $\overline{f}^{(1)}$ was computed for the boundaries of the outer segment, located at $z_{\rm OS,0}$ and 4 pixels deeper (corresponding to about 28 μ m in air and 20 μ m in tissue) at $z_{\rm OS,1}$ (see also Fig. 2a). Finally, the phase difference between both boundaries of the outer segment was obtained by

$$f_{xyt}^{(2)} = \overline{f}_{xyz_{OS,0}}^{(1)} \overline{f}_{xyz_{OS,1}}^{(1)*}$$

The signal quality was improved by applying a lateral Gaussian filter to the complex data $f_{xyt}^{(2)}$ ($\sigma = 16\,\mathrm{px}$, Fig. 2, Fig. 3) or a moving average filter over 15 volumes (Fig. 4).

For strong signals, where the phase signal $\Delta \phi_{xyt} = \arg f_{xyt}^{(2)}$ exceeded π (Fig. 4), the phases were unwrapped temporally (Fig. 3l and Fig. 4). Phases were finally converted into optical thickness changes using

$$\Delta \ell = \frac{\Delta \phi}{4\pi} \lambda_0$$
,

where λ_0 is the central wavelength of the OCT system, i.e., $\lambda_0 \approx 841$ nm, and $\Delta \phi = \arg f^{(2)}$ is the phase change.

Acknowledgements

We would like to thank Reginal Birngruber and Alfred Vogel for valuable discussions on the results, and Hans-Jürgen Rode, Jörn Wollenzin, and Christian Winter for their help with the electronics setup.

This research was sponsored by the German Federal Ministry of Education and Research (Innovative Imaging & Intervention in early AMD, contract numbers 98729873C and 98729873E).

Author contributions

D.H. and G.H. had the initial idea. D.H. worked on the setup, collected, analyzed, and interpreted the data, helped obtain funding, and wrote the manuscript. H.Sp. worked on the setup and collected data. C.P. worked on the setup, collected and

interpreted the data. H.Su. and G.F. worked on the setup. G.H. obtained funding and interpreted the data.

Competing financial interests

D.H. is working for Thorlabs GmbH, which produces and sells OCT systems. D.H. and G.H. are listed as inventors on a related patent application (application no. PCT/EP2012/001639). All other authors declare no competing financial interests.

References

- ¹ Liebman, P. A., Jagger, W. S. & M. W. Kaplan, F. G. B. Membrane structure changes in rod outer segment associated with rhodopsin bleaching. *Nature* **251**, 31–36 (1974).
- ² Harary, H., Brown, J. & Pinto, L. Rapid light-induced changes in near infrared transmission of rods in bufo marinus. *Science* **202**, 1083–1085 (1978).
- ³ Yao, X. & Wang, B. Intrinsic optical signal imaging of retinal physiology: a review. *J. Biomed. Opt.* **20**, 090901 (2015).
- ⁴ Jonnal, R. S. *et al.* In vivo functional imaging of human cone photoreceptors. *Opt. Express* **15**, 16141–16160 (2007).
- ⁵ Grieve, K. & Roorda, A. Intrinsic signals from human cone photoreceptors. *Invest. Ophthalmol. Vis. Sci.* **49**, 713 (2008).
- ⁶ Srinivasan, V. J., Chen, Y., Duker, J. S. & Fujimoto, J. G. In vivo functional imaging of intrinsic scattering changes in the human retina with high-speed ultrahigh resolution OCT. *Opt. Express* 17, 3861–3877 (2009).
- ⁷ Schmoll, T., Kolbitsch, C. & Leitgeb, R. A. In vivo functional retinal optical coherence tomography. *J. Biomed. Opt.* **15**, 041513–041513–8 (2010).
- ⁸ Teussink, M. M. *et al.* Impact of motion-associated noise on intrinsic optical signal imaging in humans with optical coherence tomography. *Biomed. Opt. Express* **6**, 1632–1647 (2015).

- ⁹ Huang, D. *et al.* Optical coherence tomography. *Science* **254**, 1178–1181 (1991).
- ¹⁰ Bizheva, K. et al. Optophysiology: depthresolved probing of retinal physiology with functional ultrahigh-resolution optical coherence tomography. Proc. Natl. Acad. Sci. U. S. A. 103, 5066– 5071 (2006).
- ¹¹ Srinivasan, V. J., Wojtkowski, M., Fujimoto, J. G. & Duker, J. S. In vivo measurement of retinal physiology with high-speed ultrahigh-resolution optical coherence tomography. *Opt. Lett.* 31, 2308–2310 (2006).
- ¹² Hillmann, D., Lührs, C., Bonin, T., Koch, P. & Hüttmann, G. Holoscopy holographic optical coherence tomography. *Opt. Lett.* **36**, 2390–2392 (2011).
- ¹³ Považay, B. *et al.* Full-field time-encoded frequency-domain optical coherence tomography. *Opt. Express* **14**, 7661–7669 (2006).
- ¹⁴ Bonin, T., Franke, G., Hagen-Eggert, M., Koch, P. & Hüttmann, G. In vivo Fourier-domain full-field OCT of the human retina with 1.5 million A-lines/s. *Opt. Lett.* **35**, 3432–3434 (2010).
- ¹⁵ Spahr, H. *et al.* Imaging pulse wave propagation in human retinal vessels using full-field swept-source optical coherence tomography. *Opt. Lett.* **40**, 4771–4774 (2015).
- ¹⁶ Adie, S. G., Graf, B. W., Ahmad, A., Carney, P. S. & Boppart, S. A. Computational adaptive optics for broadband optical interferometric tomography of biological tissue. *Proc. Natl. Acad. Sci. U.S.A.* 109, 7175–7180 (2012).
- ¹⁷ Shemonski, N. D. *et al.* Computational high-resolution optical imaging of the living human retina. *Nature Photon.* **9**, 440–443 (2015).
- ¹⁸ Hillmann, D. *et al.* Aberration-free volumetric high-speed imaging of in vivo retina. Submitted to *Sci. Rep.* (2015).
- ¹⁹ Uhl, R., Hofmann, K. P. & Kreutz, W. Measurement of fast light-induced disc shrinkage within bovine rod outer segments by means of a light-scattering transient. *Biochim. Biophys. Acta* 469, 113–122 (1977).

- ²⁰ Müller, H. H. *et al.* Imaging thermal expansion and retinal tissue changes during photocoagulation by high speed OCT. *Biomed. Opt. Express* **3**, 1025–1046 (2012).
- ²¹ Lamb, T. D. Gain and kinetics of activation in the G-protein cascade of phototransduction. *Proc. Natl. Acad. Sci. U.S.A.* **93**, 566–570 (1996).
- ²² Curcio, C. A., Medeiros, N. E. & Millican, C. L. Photoreceptor loss in age-related macular degeneration. *Invest. Ophthalmol. Vis. Sci.* 37, 1236 (1996).
- ²³ Nagy, D., Schönfisch, B., Zrenner, E. & Jägle, H. Long-term follow-up of retinitis pigmentosa patients with multifocal electroretinography. *Invest. Ophthalmol. Vis. Sci.* 49, 4664 (2008).
- ²⁴ Archibald, N. K., Clarke, M. P., Mosimann, U. P. & Burn, D. J. The retina in Parkinson's disease. *Brain* **132**, 1128–1145 (2009).
- ²⁵ Williams, P. A. *et al.* Retinal ganglion cell dendritic degeneration in a mouse model of Alzheimer's disease. *Neurobiol. Aging* **34**, 1799 1806 (2013).
- ²⁶ Wojtkowski, M. *et al.* Ultrahigh-resolution, high-speed, Fourier domain optical coherence tomography and methods for dispersion compensation. *Opt. Express* **12**, 2404–2422 (2004).
- ²⁷ Fienup, J. R. Synthetic-aperture radar autofocus by maximizing sharpness. *Opt. Lett.* **25**, 221–223 (2000).